Leveraging smart lights for passive localization

Wang, Weizheng; Zhang, Junwei; Wang, Qing; Zuniga, Marco

DOI
10.1109/MASS.2018.00049

Publication date
2018

Document Version
Final published version

Published in
2018 IEEE 15th International Conference on Mobile Ad Hoc and Sensor Systems (MASS)

2018 IEEE 15th International Conference on Mobile Ad-hoc and Sensor Systems

Leveraging Smart Lights for Passive Localization

Weizheng Wang[1], Junwei Zhang[1], Qing Wang[2], and Marco Zuniga[1]
[1]TU Delft, the Netherlands [2]KU Leuven, Belgium
Email: w.wang-14@tudelft.nl qing.wang@kuleuven.be m.a.zunigazamalloa@tudelft.nl

***Abstract*—Localization based on visible light is gaining significant attention. But most existing studies rely on a key requirement: the object of interest needs to carry an optical receiver (camera or photodiode). We remove this requirement and investigate the possibility of achieving accurate localization in a *passive* manner, that is, without requiring objects to carry any optical receiver. To achieve this goal, *we exploit the reflective surfaces of objects* and the unique propagation properties of LED luminaires. We present geometric models, a testbed implementation, and empirical evaluations to showcase the opportunities and challenges posed by this new type of localization. Overall, we show that our method can track with high accuracy (few centimeters) a subset of an object's trajectory and it can also identify passively the object's ID.**

I. Introduction

Thanks to advances in the area of Visible Light Communication (VLC), we now have the ability to piggyback wireless communication on top of LED illumination. This technological breakthrough is creating a new range of exciting applications: localization [1], Internet connectivity via luminaires [2], and a new generation of interactive toys [3], to name a few. Among these applications, localization is arguably one of the areas that is benefiting the most. This is due to the fact that visible light waves have propagation properties that are well suited for estimating range: they attenuate in a smooth and rather deterministic manner. For example, when simple trilateration methods are used with radio frequency signals such as WiFi –which are notorious for having severe multipath effects–, the localization accuracy is between 2 m and 6 m [4]. But the same trilateration methods provide sub-meter accuracy when VLC-enabled luminaires are used as anchor emitting beacons [5].

Research problem. Current localization methods based on VLC [5], [6] provide high accuracy but share an important constraint: they require objects to carry photosensors to decode the beacons sent by luminaires. We remove this constraint and investigate passive VLC-localization, that is, localization in scenarios where the object of interest does not carry any photosensor. The case we make to investigate *passive* localization is simple: when objects do not carry photosensors, the only areas that are *constantly* exposed to light are their external surfaces, thus, it's important to *investigate the interaction between VLC luminaires and the reflections coming from these external surfaces to identify cues for localization*. Considering this type of scenarios, we want to understand under what conditions would such a localization system work and what would the expected accuracy be.

Fig. 1 captures the limitations of a naive implementation of passive localization with visible light. Consider two luminaires

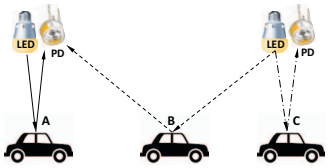

Fig. 1. The concept of passive localization with smart lights.

that send periodic beacons $\mathcal{L}_1$ and $\mathcal{L}_2$. Each luminaire has a photodiode (PD) attached to it. In general, the PDs co-located with the luminaires may not be able to hear those beacons back due to the low reflectivity of ground surfaces. But if a mobile object with a high reflective surface passes by, the PDs will receive their own (or a neighboring) beacon, and thus, be able to detect the presence of the object. For example, if luminaire $\mathcal{L}_1$ hears its own beacon, it will infer that an object is in region A, and if it hears a beacon from luminaire $\mathcal{L}_2$, it will infer that an object is in region B. But this basic configuration has three drawbacks: *poor coverage*, few positions can be detected (regions A, B and C in this case); *coarse grained accuracy*, the exact location of the object cannot be determined because we do not know the reflecting angles (shape) of the object; and *there is no identification*, this system can only determine the presence of an object but not its ID, if more than one object is present, the objects cannot be distinguished.

Passive VLC localization could be applied to scenarios where objects move on established paths in illuminated areas, e.g. mining tunnels or underground train and vehicular systems. In those underground scenarios, radio-based solutions face severe multipath effects, rendering most of those approaches inaccurate.

Our contributions. We propose a novel *passive* localization system to overcome the above described limitations. Our contributions in this new area are listed below:

1) *Geometric model for localization* (Section II). We develop a geometric model to identify guidelines for the proper design of the transmitters (luminaires), improve the detection coverage, and increase the localization accuracy.
2) *Passive identification* (Section III). To identify the objects moving under the luminaires, we embed barcode-like IDs onto the objects' surfaces, and propose a novel framework to decode these IDs via passive reflections.
3) *Implementation* (Section IV). We design and implement a testbed to evaluate our system. To test short-range scenarios, we modify an open platform. For medium-range scenarios, we develop our own VLC transmitters using standard off-the-shelf LED bulbs.

2155-6814/18/$31.00 ©2018 IEEE
DOI 10.1109/MASS.2018.00049

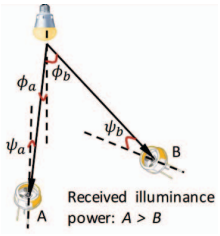

Fig. 2. The Lambertian model.

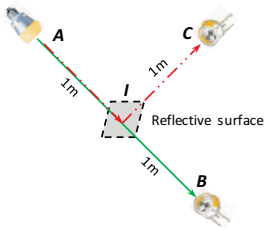

Fig. 3. Capture of reflection effect.

4) *Evaluation* (Section V). We evaluate our system under three different scenarios with increasing levels of complexity. Our results show that we can pinpoint with cm accuracy a subset of the object's trajectory and we are able to identify the object's ID in a passive manner.

II. Model for Passive Localization

To gain a better understanding about the properties and limitations of passive localization with visible light, we use two models: the Lambertian source, which models the radiation pattern of LED lights; and a geometric model based on the laws of reflection. In the rest of this paper, we focus on one-dimensional topologies and assume that (i) *LED luminaires are VLC transceivers* (they can transmit information by modulating their light intensity and they have a photodiode to receive VLC packets), and (ii) the reflective coefficient of objects is higher than that of the surface where the object is moving on.

A. Detecting objects without line-of-sight

In VLC, angles play a major role on the received illuminance power. Fig. 2 captures this behaviour. The wider the irradiation angle ϕ and the wider the incidence angle ψ, the lower the received illuminance. Also, depending on the LED's optical enclosure, the radiation beam can be long and narrow, or broad and short. Formally, these relationships are captured by the well known Lambertian model H. Denoting P_t as the illuminance power of the LED, the received illuminance power P_r at the photosensor is given by:

$$P_r = P_t \cdot H \tag{1}$$

where

$$H = \begin{cases} \frac{(m+1)A}{2\pi d^2} \cos^m \phi T(\psi) g(\psi) \cos(\psi), & 0 \le \psi \le \Psi_c \\ 0, & \psi > \Psi_c \end{cases} \tag{2}$$

where m is the lambertian order determining the width and length of the beam, a higher m leads to a longer and narrower beam; d is the distance between the LED and the photosensor; A is the detecting area of the photosensor; $T(\psi)$ and $g(\psi)$ are the concentrator and filter gains at the photosensor; and Ψ_c is the field-of-view of the receiver.

The Lambertian model however is meant for line-of-sight communication. Passive localization relies on reflected beams (no-line-of-sight). To capture the effect of reflections, we modify the above equation based on two properties of the reflective surface; its area A_s and its reflective coefficient ρ.

$$H_{\text{NLOS}} = H f(A_s) \rho \tag{3}$$

TABLE I
Measured combined coefficient ρ of different materials

Material	Mirror	Aluminum	White cardboard
Coefficient ρ	0.89	0.62	0.30

where $f(A_s)$ is a linear function of A_s, as explained later. To capture the effect of these two new parameters, we perform the following experiment. First, we set a transmitter and a receiver at a two-meter distance with line-of-sight, as shown in Fig. 3, points A and B. Then we put a reflective surface at point I, one meter away from the LED, and move the receiver to point C (mirror image of point B). In this experiment we change the area (A_s) and the material (ρ) of the reflective surface. Our results lead to a design guideline for passive localization.

Guideline 1: *The reflective surface of the moving object A_s should be at least the same size as the receiver's area A.* Fig. 4 depicts the effect of changing the area of the reflective surface. For these experiments we use mirrors as the reflecting surface. When the area is small, the received illuminance power is low. Beyond a point however further increasing the area of the reflective surface does not increase the received illuminance power. This occurs because, with specular reflections, the majority of reflections caused by larger areas do not reach the receiver. Thus, a reflective surface that is smaller than the photosensor's surface affects coverage, because it reduces the likelihood of detecting the object.

B. Achieving full coverage

The previous subsection indicates that an object only requires a small reflective area to be localized. But this approach only provides limited coverage. In the simplest case, considering N luminaires we would only be able to identify $2N-1$ points. The N points under the luminaires and the $N-1$ intermediate points. However, since the size of the reflective surface can be small, an object can carry an array consisting of many small reflecting surfaces but tilted at different angles. The different angles will reflect beams towards the receiver at different locations, improving coverage. Based on simple geometry, we can make the following propositions.

Proposition 1. *Given two neighboring luminaires i and j, with an inter-distance d and height h from the ground; for any given position x between the lights, there is a tilted angle that will reflect light towards a neighboring transceiver:*

$$\alpha_{ij} = \frac{\arctan(\frac{d-x}{h}) - \arctan(\frac{x}{h})}{2}$$

where clockwise turns denote positive direction of angles.

Based on Proposition 1, we can get:

Proposition 2. *For a given position x, there always exists a tilted angle that can make the object reflect light back towards the same transceiver:*

$$\alpha_{ii} = -\arctan(\frac{x}{h}), \qquad \alpha_{jj} = \arctan(\frac{d-x}{h}) \tag{4}$$

Guideline 2: *A small polyhedral-reflector can be added on top of the object to provide constant coverage.* Consider an object with a reflective coefficient that is too low to reflect

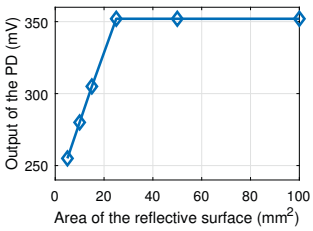

Fig. 4. Impact of the area of the reflective surface (used material is mirror).

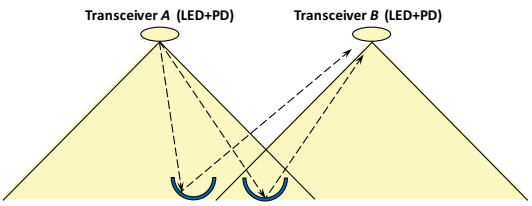

Fig. 5. The problem of unique signature when each transceiver has a single beam *(the object has many tiny reflective surfaces titled at different angles (kind of 'retro-reflector') to improve the coverage)*

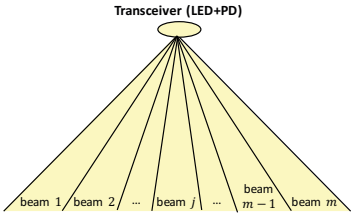

Fig. 6. A transmitter with m beams *(here we use a triangle instead of the Lambertian shape to represent the coverage of an LED, for simplicity.)*

a VLC message. Such an object could not be localized in our system. To solve this problem, we can add polyhedral-reflectors to provide better coverage. A polyhedral-reflector can be created to reflect a wide incoming beam (cm^2) into many outgoing narrow beams (mm^2) in different directions. Note that even if an object has a high reflective coefficient, a polyhedral-reflector can be still used to increase coverage, since few objects have surfaces with multiple tilted angles.

C. Obtaining unique signatures

Until now, our guidelines have focused on the issue of coverage (i.e. increase the number of detected points). But we have not tackled the issue of obtaining a unique fingerprint for each detected point. To highlight this problem, let us use Fig. 5. Luminaire B receives the *same* beacon for the two positions of the convex surface, and thus, it cannot pinpoint the exact location. One way to discern two locations with the same beacon-ID is to use the RSS. But due to the intricate relation among the irradiation and incident angles, the lambertian order m and the distance traveled d; we observed two problems. First, except for a few points, most RSS values map to multiple locations. Second, the sensitivity of simple photodiodes is not sufficient to distinguish small changes in RSS.

Due to the limitations of RSS, we propose to use luminaires with multiple beams, as shown in Fig. 6. Instead of having a single *wide* beam with a low lambertian order, we propose to use multiple *narrow* beams with higher lambertian order. Notice that the overall power does not need to increase, since each narrow beam requires less energy to attain the same range as a wide beam. In our system, each beam emits a unique ID tuple $< \mathcal{L}, \mathcal{B} >$, where $\mathcal{L}$ denotes the ID of the luminaire and $\mathcal{B}$ the ID of the beam within that luminaire.

Guideline 3: *Luminaires should be designed with multiple beams, the more beams the better.* It is important to highlight that standard off-the-shelf LED lights already consist of multiple internal LED substrates. Many of these LED substrates point to different directions. Designing VLC luminaires for passive localization would entail adjusting the angles of some of these beams and providing each beam with a unique ID $\mathcal{B}$.

D. Localization algorithm

Assuming a set of luminaires and objects following our guidelines, the localization algorithm works as follows.

Step 1: The algorithm requires as inputs: the inter-node distance d, the height of luminaires h, the FoV of the photosensor ω, the number of beams at each luminaire b, a vector μ with the directional angles of the beams, and a vector containing the k tilted angles of the reflector (surface) $\{\alpha_1, \ldots, \alpha_k\}$.

Step 2: Using Proposition 1, the transceiver calculates the locations $\hat{x_i}$ for all the tilted angles $\alpha_i, i = 1, \ldots, k$. At this point we have k possible locations for the moving object.

Step 3: Upon receiving a beacon from a neighboring light, or from itself, the algorithm computes the region covered by that beam: $[x^1_{\mathcal{L}.\mathcal{B}}, x^2_{\mathcal{L}.\mathcal{B}}] = [h\tan(\mu_{\mathcal{L}.\mathcal{B}} - \omega/2), h\tan(\mu_{\mathcal{L}.\mathcal{B}} + \omega/2)]$. At this point we know the object is under the coverage of beam $< \mathcal{L}.\mathcal{B} >$, but we do not know exactly where.

Step 4: The only valid locations $\hat{x_i}$ (Step 2) are those that fall in the range $[x^1_{\mathcal{L}.\mathcal{B}}, x^2_{\mathcal{L}.\mathcal{B}}]$ (Step 3). If only one estimation $\hat{x_i}$ falls in this range, $\hat{x_i}$ is given as the object's location. If multiple estimations fall in the range, the algorithm either returns the average as the location, or chooses one of the estimations with higher probability if the direction and velocity of the target can be estimated with prior points.

III. Passive Identification

Localizing an object is not enough. We now introduce how to further *identify* the object *passively* in our system.

Our approach is inspired by a recent work that leverages ambient light for passive communication [7], which adopts the patterns of distinctive reflecting surfaces to modulate ambient light. In this paper, we use a similar method to label objects with unique IDs attached to objects' surface, as illustrated in Fig. 7. We refer to this 'barcode' as *object-ID*. We use materials with different reflection coefficients to build an object-ID, e.g, aluminium (high) and black paper (low). To decode an object-ID at the PD according to the light it reflects, we have to tackle two challenges:

- *Overlapping signals containing the beam-ID and object-ID.* As presented in Sec. II, each transmitter sends modulated light containing its *beam-ID*. At certain positions, this modulated light can be *reflected* by the object's surface to the PD and be used to localize the object. But the *object-ID* also *modulates* the impinging light, albeit at a lower frequency. Thus, the PD will receive an overlapping signal containing both the beam-ID and the object-ID, as illustrated in Fig. 8. To identify the object, we need to extract the signal that only contains the object-ID from the overlapping signal.
- *Inter-Symbol Interference (ISI).* At some positions, different parts of the object-ID can reflect concurrently the

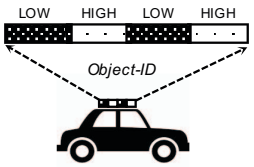

Fig. 7. Attach barcode-like ID to the surface of the object

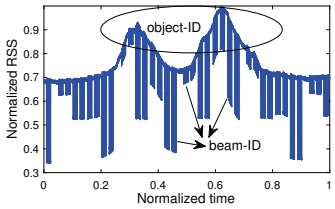

Fig. 8. Illustration of the overlapped signal

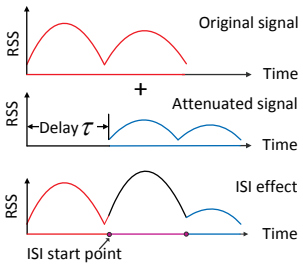

Fig. 9. Illustration of the inter-symbol interference

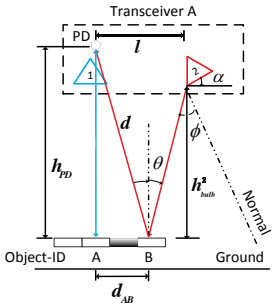

Fig. 10. Illustration of the geometric model used to remove the ISI

light coming from two neighbouring beams. Therefore, the light modulated by the object-ID may contain interference caused by itself, namely, an ISI effect. As illustrated in Fig. 10, the lights of beam-1 and beam-2 are modulated by the third symbol (at point A) and the first symbol (at point B) of the object-ID, respectively. This generates ISI at the PD, as shown in Fig. 9. Assuming that the object traverses point A first, then the signal modulated at point B is *actually an attenuated and delayed* version of the original modulated signal at point A. In the rest of this paper, we refer to these two types of signals as *attenuated signal* and *original signal*, respectively.

A. Decoupling of overlapping signals

We tackle this problem by proposing a downsampling-based method motivated by the following observations: *(i)* The signal containing the beam-ID is a *high-frequency signal* (created by modulating LEDs at high speed) while the signal containing the object-ID is a *low-frequency signal* (created by the object's movement); *(ii)* When the LED transmits OFF symbols (namely, LED is off), there is a drop in the signal intensity received at the PD, as shown in Fig. 8. However, when transmitting ON symbols (namely, LED is on), no drop exits. *In other words, the overlapping signal only occurs when OFF symbols are transmitted. Thus, we just need to remove the OFF symbols from the overlapped signals.*

The proposed down sampling method works as follows: *(i)* Guarantee that there are no continuous OFF symbols in the modulated data at the LEDs (this is a necessary requirement to remove the OFF symbols in our method). To achieve this, we use the following modulation at transceivers: use a symbol sequence of OFF-ON to denote a bit 0, and symbol sequence of OFF-ON-ON to denote a bit 1; *(ii)* Set the downsampling interval slightly wider than the duration of an OFF symbol. By doing this, we guarantee that each OFF symbol is sampled at most once; *(iii)* Compare each two adjacent samples: if the difference of two adjacent samples is higher than a threshold (i.e., an abrupt drop occurs in the RSS), then we discard the sample that has a lower value (i.e., remove the OFF symbol).

B. Remove the inter-symbol interference

To eliminate the effect of ISI, we propose a method to remove the attenuated signal from the original one. To do this, we need the following information: (1) the *delay* of the attenuated signal with respect to the original signal; and (2) the *intensity* of the attenuated signal. Next we present how to obtain these information and how to extract and decode the original signal after that.

1) Obtaining the delay of the attenuated signal: Consider the scenario in Fig. 10. As presented earlier in this section, the ISI starts when the object reaches point B. At this position, a symbol (e.g., the ith symbol) of the object-ID will generate interference by modulating the light emitted by beam-2. *Note that this modulated light contains the ID of beam-2 and this beam-ID can be decoded by the PD for localization.* Moreover, when reaching point A, this ith symbol has modulated the light emitted by beam-1, and this modulated light carrying the ID of beam-1 has been decoded by the PD as well.

Let t_0 and $t_0+\tau$ be the time when *for the first time* the PD decodes the IDs of beam-1 and beam-2, respectively. Since the transceiver can modulate light at a very high speed (i.e., it can transmit the frames that contain beam-IDs very frequently), *we can assume that t_0 and $t_0+\tau$ are the time when the object reaches point A and point B, respectively.*

Therefore, *the difference between t_0 and $t_0+\tau$, namely, τ, is the delay of the attenuated signal.* Note that t_0 and $t_0+\tau$ can be obtained easily in practice. Besides, at some positions (as will be presented in Sec. V-C), τ can be a *negative* value, meaning that the attenuated signal starts *earlier* than the original signal.

2) Obtaining the intensity of the attenuated signal: To derive this, we still use Fig. 10 as an illustration. Let h_{PD} and h^2_{bulb} denote the heights of the PD and bulb 2, respectively, and let l be the horizontal distance between them. From the geometric model in Fig. 10, we can derive the distance d_{AB}

$$d_{\text{AB}} = l \cdot h_{\text{PD}} / \left(h_{\text{PD}} + h^2_{\text{bulb}}\right) \tag{5}$$

Let θ and ϕ be the reflection angle at point B and irradiance angle of bulb 2, respectively. We have $\theta = \arctan \frac{d_{\text{AB}}}{h_{\text{PD}}}$ and $\phi = \alpha + \theta$. Based on Eq. (1), we can obtain the intensity of the attenuated signal modulated by the object-ID at point B:

$$P^B_{\text{att}} = \frac{\rho P_t (m+1) cos^m(\phi)}{2\pi d^4} T(\theta) g(\theta) cos(\theta) \tag{6}$$

Similarly, the intensity of the original signal modulated by the object-ID at point A can be expressed as follows:

$$P^A_{\text{orig}} = \frac{\rho P_t (m+1) cos^m(0)}{2\pi h^4_{\text{PD}}} T(0) g(0) cos(0) \tag{7}$$

In our model, we can assume that $h_{\text{PD}} \approx h_{\text{bulb}}^2 \gg l$. Then we have the approximation: $h_{\text{PD}} \approx d$. Besides, there is no optical filter or concentrator in our system. Thus, $T(\cdot)$ and $g(\cdot)$ are constant in our model. Let η denote the *attenuation ratio*, defined as the ratio between the intensity of the attenuated signal and that of the original signal, then we have

$$\eta = P_{\text{att}}^B / P_{\text{orig}}^A = cos^m(\phi)cos(\theta) \tag{8}$$

3) Extract and decode the original signal: To achieve this, from now on we consider the continuous version of the signals. Following convention, we use $f(t)$ to denote a continuous signal. Let $f_{\text{orig}}(t)$ and $f_{\text{att}}(t)$ be the continuous original signal and the continuous attenuated signal, respectively. We have

$$f_{\text{att}}(t) = \eta f_{\text{orig}}(t - \tau) \tag{9}$$

Let $f_{\text{sum}}(t)$ be the aggregated signal received at the PD, then

$$f_{\text{orig}}(t) = f_{\text{sum}}(t) - f_{\text{att}}(t) = f_{\text{sum}}(t) - \eta f_{\text{orig}}(t - \tau) \tag{10}$$

As presented in Sec. III-B1, we can denote t_0 as the time when the object-ID reaches point A and $t_0 + \tau$ as the time when the object-ID reaches point B where the ISI appears. Since there is no ISI during the time slot $[t_0, t_0 + \tau)$, we have

$$f_{\text{orig}}(t) = f_{\text{sum}}(t), \quad \forall t \in [t_0, t_0 + \tau) \tag{11}$$

Based on Eq. (10) and Eq. (11), we can now obtain the original signal $f_{\text{orig}}(t)$ (without the ISI effect). To decode it, we use a simple threshold-based decoding method (omitted due to its simplicity, limited novelty, and the page limitation).

IV. Testbed

A solid evaluation of passive localization with VLC requires designing a system where multiple parameters can be adjusted. Below we describe how we use our design guidelines to build a comprehensive evaluation testbed.

A. Luminaire design

We design our luminaires based on the Shine platform [8]. We extend it largely in both the hardware and software to build our testbed in three ways. First, we improve its reception capabilities, a front-end we refer to as *Shine+*. Second, we add more powerful LEDs to build another front-end referred as *Shine++*. Third, we modify its software. The block diagram of our new testbed is given in Fig. 11. Next, we present the design details of both front-ends.

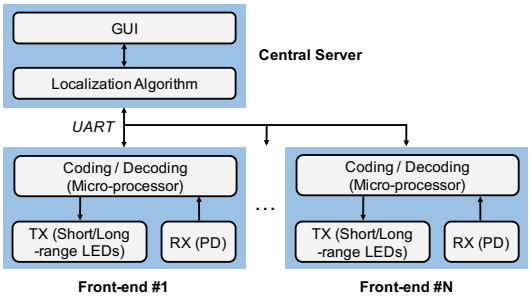

Fig. 11. The function blocks of our redesigned testbed

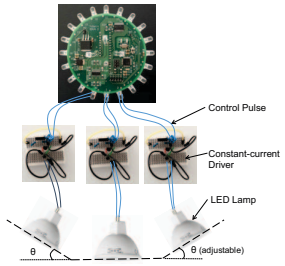

Fig. 12. Our testbed with the front-end Shine++

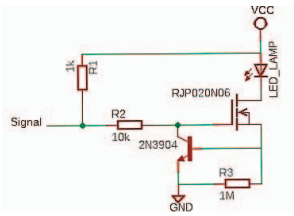

Fig. 13. The driver circuit for the high-power LED bulb in Shine++

*1) **A short-range luminaire with multiple-beams – Shine+**:* Shine has multiple narrow beams, which follows *Guideline 3*, but it is designed for line-of-sight communication. Since we rely on *non-line-of-sight reflections*, we must improve Shine's reception capabilities. To achieve this goal, we implement two changes. First, we change the PD from SFH203P to SFH206K, which extend the communication range by 165%. Second, we add a low pass filter to improve the signal-to-noise ratio.

*2) **A medium-range luminaire with less-beams – Shine++**:* To evaluate our sensing approach with longer ranges, we build a new front-end with commercial LED bulbs, dubbed Shine++. We choose the IKEA Ledare LED with a viewing angle of 36 °as the transmitters. Each LED consumes 3.5 W, thus we design a new LED driver circuit to provide higher power, as shown in Fig. 13. We use three LED bulbs, one placed in the middle and the other two on the sides with adjustable inclination angles, as shown in Fig. 12.

*3) **Software**:* Our SW implements the data transmission and reception, the access control for the shared visible light medium, the localization and object identification algorithms.

In our application we need accurate timing to schedule the modulation of light beams. We connect all the nodes to a central server (PC/laptop), where we run a Time Division Multiple Access (TDMA) scheme. This scheme turns *on* all LEDs, but modulates only one *beam* at a time. Adaptive decoding thresholds are implemented in our system to eliminate interference from external light sources, including neighboring LEDs that are *on* but not modulated. The MAC schedules the LEDs 'remotely' through the interface with the micro-controllers. Similarly, the data received from the PDs are decoded at the micro-controllers and sent through the UART to the central server. Upon receiving these frames, the server runs the *localization algorithm* (cf. Section II-D) and calculates on-the-fly the current position of the mobile object. The outcome of the algorithm is demonstrated in a simple GUI (omitted due to the space limitation).

B. Object design

For passive localization with VLC, the external surface of the objects plays a key role. Three out of the four guidelines in Section II pertain to the object's surface. In this subsection we describe the surfaces we use for our evaluation and the reasoning behind selecting them.

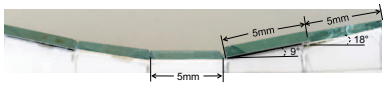

Fig. 14. Side view of the object with *perfect* reflective coefficient

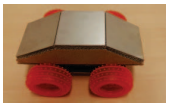

Fig. 15. Customized toy car *(standard reflector, 28cm×11cm×7cm)*

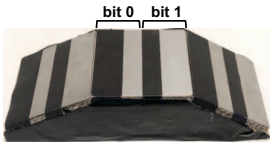

Fig. 16. The object-ID "10" that is attached to all the three parts of the object

1) ***A perfect reflector****:* As stated by our guidelines, the ideal surface would use materials with very high reflective coefficients and specular reflection to enable non-line-of-sight communication, and would consist of small reflecting areas (Guideline 1) tilted at different angles (Guideline 2) to increase coverage. We use thin strips of flat mirrors to satisfy these three guidelines. Fig. 14 presents a side view of the reflecting object, which consists of five mirrors with inclined angles of -18°, -9°, 0°, 9°, 18°, respectively. All the mirrors have the same width of 5 mm.

2) ***A standard reflector****:* To evaluate the performance of passive localization with more standard objects, we use a customized toy car. Such an object relaxes the requirements of our first three guidelines. The material is metal, whose reflective coefficient is not as good as mirrors. Second, the surfaces are big (relaxes Guideline 1). Third, it has few tilted angles (relaxes Guideline 2). For our object, we consider three parts of a car: the front windshield, the roof, and the back windshield. After a thorough investigation of different cars' shapes, we decide to customize a toy car with inclined angels of -30°, 0°, 25°. The final customized car is shown in Fig. 15. Note that we are aware of the fact that different parts of a real car have different reflection coefficients, but we only use one type of material for a single toy car in this work for simplicity. We build two different toy cars, one with aluminum and the other one with mirrors.

3) ***Design of object-ID****:* We label the objects in our system with unique IDs consisting of certain patterns. We use 3cm-width metal (high reflection coefficient) and 2cm-width black tissue (low reflection coefficient) to represent a bit 1, and use 2cm-width of metal and 3cm-width of black tissue to represent a bit 0. An object-ID for "10" is shown in Fig. 16 where it is attached to all the three faces of the customized toy car.

V. Evaluation

In this section, we evaluate our methods under increasingly complex test cases. First we present the evaluation on localization, followed by the evaluation on identification. Note that our passive localization and identification methods can work at the same time, as described in Sec. V-C.

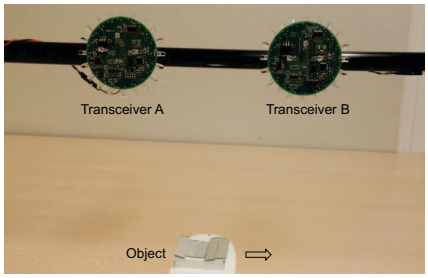

Fig. 17. Experiment setup in the ideal case (height=15 cm, inter-node distance=20 cm)

A. Localization: ideal case

For the ideal case we use the best possible setup: the front-end with many beams (Shine+) together with the perfect reflector. The experiment setup is shown in Fig. 17. We deploy two nodes (denoted as A and B) at an inter-node distance of 20 cm, and at a height of 15 cm from a desktop. Shine+ can achieve reliable VLC at a distance of up to 50 cm. By deploying the two nodes as described above, we can assure that the distance travelled by the reflected signals is shorter than the maximal communication distance (i.e., 50 cm). It is also important to highlight that the angles of the perfect reflector are designed based on Propositions 1 and 2 to guarantee that every beam has at least one angle that will reflect the light to a neighboring node or to itself. If these angles are not selected carefully, the system may end up having beams without reflections, and thus, no localization could be performed inside the area covered by these beams. Different inter-node distances or heights will lead to different tilted angles.

Results. The evaluation results are shown in Fig. 18. The red dots represent the ground truth. The experiments were repeated ten times and we did not observe any major variance, which is expected due to the rather deterministic propagation properties of light waves and the nearly specular reflection of mirrors. We can observe that the results from our algorithm match well the ground truth. Nearly half of the locations are localized with almost perfect accuracy, while the other locations are detected with errors up to 1.3 cm.

The detail on how these locations are detected is given in Table. II. Now let us give some more insights on how our algorithm (cf. II-D) leads to these results. The object moves from left to right. The algorithm has all the inputs required in Step 1. The first detected point *R1* is a self reflection, i.e., transceiver A receives the reflection of beam *A.2*. The server calculates all the ground truth locations that the set of self-reflecting angles $\{\alpha_1, \ldots, \alpha_k\}$ can have (Step 2). Then it calculates the valid region for this beam *A.2* (Step 3). The algorithm detects that only one point falls in the valid region, and hence, reports that point as the estimated location. The true location is $\approx$1 cm to the right. The next two estimated locations, *R2* and *R3*, are also self-reflections. The fourth estimated location *R4* is due to the communication between transceivers A and B (inter-node reflection). Notice that in this case, two locations are within the valid region of beam

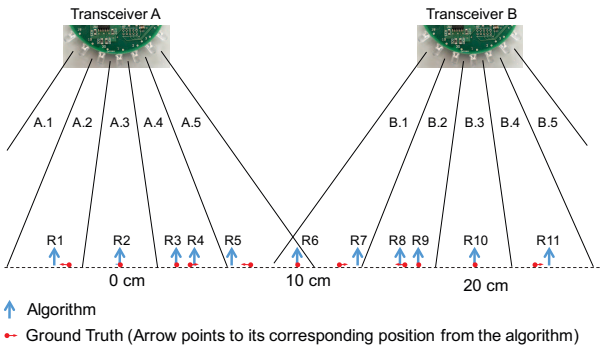

Fig. 18. Evaluation results in the ideal case

TABLE II
DETAILS OF THE LOCALIZED POSITIONS FROM OUR ALGORITHM
(No.: the detected locations; TX: transmitter; RX: receiver)

No.	R1	R2	R3	R4	R5	R6	R7	R8	R9	R10	R11
TX	A.2	A.3	A.4	A.4	A.5	A.5	B.1	B.2	B.2	B.3	B.4
RX	A	A	A	B	B	B	A	A	B	B	B

A.4: *R3* and *R4*. But the fact that *R3* is a self reflection while *R4* is not, helps with distinguishing them. Note that *R4* does not need to be under the coverage of transceiver B to achieve inter-node reflection. This is because the photodiodes used in our experiments have a wide field of view (90^o). A more challenging case occurs with the next two locations *(R5, R6)*. These two locations are within the valid region of beam *A.5*, and both are the result of inter-node reflection. As stated in Step 4 of our algorithm, we can either average them out at the cost of increasing the error, or exploit speed and direction information from prior data to select the most likely location. We implement a very simple mechanism to exploit direction information. Every time we detect a new point we set it as the origin, prior data are given negative values based on their distance to this last point, and new data are given positive values. If two or more positive points are estimated as locations, we select the closest one (point *R5* in this case). The remainder half of the path is symmetrical to the first half, and thus, the estimation is similar to what has just been described. We don't have any location estimations for beams A.1 and B.5, because there are no self-reflecting angles for these regions. If transceiver A would have a neighbour to its left, then beam A.1 would have two potential locations (similar to *R6* and *R7*).

Regarding the errors in our estimations, we found that they are due to two main reasons. First, misalignment of the angles in the moving object, e.g. our calculations in the algorithm are done assuming the tilted angles of the object are 9^o, 18^o, etc., while in practice there are certain errors. Second, we assume that luminaires are single-LED sources, while in practice they have multiple LEDs (5 LED sources in the case of *Shine+*). This difference changes the incidence angles, which in turn affects the estimated location. This latter point is why our errors are more pronounced at the boundaries of two beams and more accurate at the center of beams.

Finally, it is important to note that passive localization with VLC operates in a fundamentally different manner compared

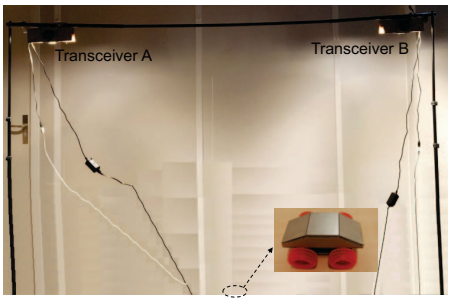

Fig. 19. Experiment setup in the realistic case

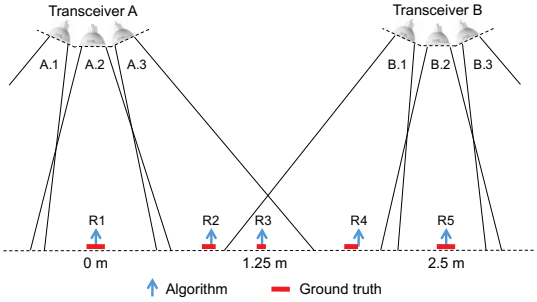

Fig. 20. Evaluation results in the realistic case (height=1.5 m, distance=2.5 m)

TABLE III
EVALUATION RESULTS (HEIGHT=1 M, INTER-NODE DISTANCE=2 M)

No.	R1	R2	R3	R4	R5
Algorithm	0 m	0.577 m	1 m	1.534 m	2 m
Mirror	-0.02∼0.02	0.63∼0.66	0.99∼1.01	1.48∼1.51	1.98∼2.02
Aluminum	-0.02∼0.02	0.62∼0.65	0.99∼1.01	1.47∼1.5	1.98∼2.02

to most localization methods. Traditionally, after a signal is received, the localization algorithm provides an estimated location that can be anywhere. In our method, the localization algorithm only has a limited number of locations to choose from. The number of locations depends on the number of beams and tilted angles. Thus, upon receiving a signal, our method's task is to map the received signal to the most appropriate location, *without requiring a training phase*.

B. Localization: realistic case

We now test our passive localization in a more realistic case, consisting of less beams and an object with less tilted angels. In this scenario, we use two nodes equipped with the Shine++ front-end. As introduced in Sec. IV, Shine++ uses more powerful LEDs, which enable nodes to communicate at a distance of 5 m In the tests, we set the height of the nodes to various levels: 1 m, 1.5 m, and 2 m.[1] Meanwhile, the inter-node distance is adjusted between 2 m and 2.5 m.

Results. The evaluation results are shown in Fig. 20, where the height and inter-node distance are set to 1.5 m and 2.5 m, respectively. For this experiment we use the aluminum-car. First, it is important to observe that in this setup we can only detect five locations, which is less than the eleven locations detected under the ideal case. This occurs because we now have less beams and less tilted angles. But all the five

[1]The height (range) can be increased if we add a lens to the photodiode.

TABLE IV
EVALUATION RESULTS (HEIGHT=1.5 M, INTER-NODE DISTANCE=2.5 M)

No.	R1	R2	R3	R4	R5
Algorithm	0 m	0.866 m	1.25 m	1.801 m	2.5 m
Mirror	-0.02∼0.02	0.85∼0.88	1.25∼1.26	1.76∼1.78	2.48∼2.52
Aluminum	-0.02∼0.02	0.85∼0.88	1.25∼1.26	1.77∼1.79	2.48∼2.52

TABLE V
EVALUATION RESULTS (HEIGHT=2 M, INTER-NODE DISTANCE=2.5 M)

No.	R1	R2	R3	R4	R5
Algorithm	0 m	1.155 m	1.25 m	1.567 m	2.5 m
Mirror	-0.02∼0.02	1.15∼1.17	1.25∼1.27	1.5∼1.52	2.48∼2.52
Aluminum	-0.02∼0.02	1.13∼1.15	none	1.51∼1.52	2.48∼2.52

estimated locations are still accurate. Note that in Fig. 20, red bars are used to represent the ground-truth positions (instead of dots as in Fig. 18). This is because the surfaces are wide enough to give a continuous location range, while in Sec. V-A the mirrors are so narrow that only a 'single' point is detected. Results under different inter-node distances and heights are given in Tables III–V. These tables show the estimations of our algorithm and the ranges of the actual locations for the aluminum- and mirror-car. From these results we can observe that the maximum localization error is around 5.3 cm and the average error is 0.97 cm. The performances with the mirror- and aluminum-car are similar. The only difference is that in Table V, the position *R3* can be detected with the mirror-car but not with the aluminum-car (due to the lower reflective coefficient of aluminum).

C. Identification

We now present the evaluation on passive identification. Without loss of generality, we use the object-ID "01" shown in Fig. 16. In the experiment, the height of the transceivers is 1.5 m and the inter-node distance is 2.5 m. The object is moved at a constant speed by hand from transceiver A to transceiver B. We only use the "standard reflector" in this test because the "perfect reflector" is too small to carry the object-ID.

Results. The signal received by the PD of transceiver A is shown in Fig. 21(a). *We clearly observe the high-frequency signal that contains the beam-ID, which has been successfully used for localization in our experiment (similar to Fig. 20).* Furthermore, we can observe that the object-ID appears three times: In Fig. 21(a), the corresponding signals are marked as *G1, G2* and *G3*. They correspond to the three positions $R1$, $R2$, and $R3$ in Fig. 20, where the object is located. Note that the PD on transceiver B captures the signals of the object-ID when the object appears at the location $R3$, $R4$, and $R5$. To decode the object-ID at these positions, we first decouple signals using the downsampling based method presented in Sec. III-A. The resulted signal is shown in Fig. 21(b), which is much cleaner. In Fig. 21(b), the first two groups of signals (*G1* and *G2*) are affected by ISI. For *G1*, which is mapped to position $R1$, ISI takes effect at the tail. For *G2* (mapped to position $R2$), ISI occurs at the beginning (τ is negative, cf. Sec. III-B1). For both *G1* and *G2*, we successfully used the steps presented in Sec. III-B to remove the ISI. The results are show in Fig. 21(c). For *G3* (mapped to position $R3$), the

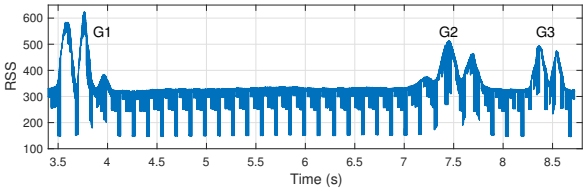

(a) Raw signal received by the PD at transceiver A

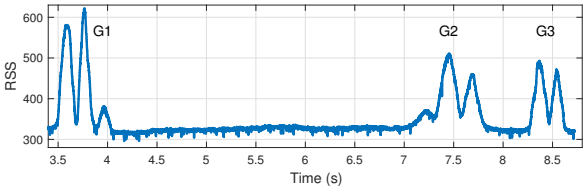

(b) Detected envelope: filtering of high-freq. signal (Sec. III-A)

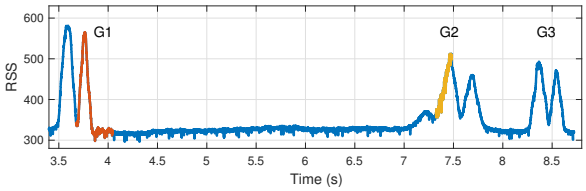

(c) After eliminating the ISI (the changes are highlighted)

Fig. 21. Performance evaluation on the passive identification

object only modulates the light of one beam. Thus, ISI does not exist, and we can decode the object-ID directly.

VI. RELATED WORK & DISCUSSION

Localization, both active and passive, has been investigated widely. In this section, we summarize the most relevant work.

Passive localization with radio. M. Youssef *et al.* introduce the concept of Device-free Passive (DfP) localization using Wi-Fi [9], [10]. They show that changes in radio signals, caused by people, can be harnessed to localize a person with an average accuracy of 0.3 m. Recently, researchers have also been able to track *multiple* objects passively with existing radio signals [11], [12]. We are motivated by these works to analyze the unique properties of visible light waves for *passive* localization. Compared to radio waves, visible light waves behave in a more deterministic manner (less multipath) but have poorer coverage (because they cannot travel through opaque objects). Our study exposes the opportunities and limitations of exploiting the external surfaces of objects to achieve accurate localization and identification.

Active localization with visible light. Epsilon [5] uses beacons sent by LED lamps and a trilateration algorithm to calculate a smartphone's position, achieving an accuracy of 0.4-0.8 m. This is improved by Luxapose [6], which leverages the angle-of-arrival of signals to achieve decimeter-level accuracy. A lighter-weight system, based on modulation via polarization, reduces the processing workload and achieves an accuracy of 3 m [13]. Complementary to existing work, LiPro deals with scenarios that only have one reference point [14]. It achieves a median error of 0.59 m by exploiting the Lambertian property of LEDs [15] and the receiver's rotation. Similar to these

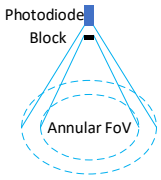

Fig. 22. Customized annular-FoV.

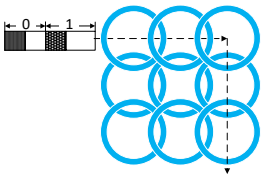

Fig. 23. 2D passive localization.

studies, we also rely on the Lambertian coverage of LED lights and the attenuation properties of visible light to obtain localization. But contrary to those studies, our method does not require the object to carry any photodetector.

Passive sensing with visible light. There is not much research on passive localization with visible light. Okuli [16] inspired our work because it uses an LED and two photodiodes to track a finger's movement with a median error of 0.7 cm within an 8x8 cm pad. Okuli exploits the fact that fingers are round and good diffusers of light to build a model-driven solution, but it requires training data and a lighting system that is *specifically designed* for near-field localization. Two other related studies are CeilingSee [17] and LocaLight [18]. CeilingSee estimates occupancy by monitoring changes in light reflection caused by people in a room. CeilingSee uses general purpose luminaries, but they require a training phase to obtain only occupancy information. LocaLight deploys photosensors on floors to track people based on the shadows they cast. Compared to our work, the main advantage of these three systems is that they do not need to modify the external surfaces of the elements they track. We, on the other hand, modify the external surfaces, but obtain accurate localization at longer ranges without requiring extra infrastructure (Okuli, LocaLight) or training phases (Okuli, CeilingSee).

Discussion. Many of the assumptions we make for the potential applications are realistic, such as knowing the height and geometry of luminaries. But our system also has limitations: (i) the path should not be bumpy, (ii) we can only track a few points in the paths, (iii) the system only works for 1-D scenarios, (iv) if multiple objects pass the same point simultaneously, they would cause 'reflection collisions', and (v) the size of the object's surface determines the maximum number of symbols that can be encoded (maximum number of IDs), (vi) the orientation of transceivers should be stable. Point (i) is a strong requirement, the bumpy spots in the detection area will generate outliers in our result. Our system is only resilient to few bumpy spots by eliminating outliers according to the object trace. The other five points can be improved. For point (ii), Kalman or Particle filters can be used to provide continuous location information. For point (iii), we can create annular FoVs with a single photodiode, cf. Fig. 22, to provide 2D localization, cf. Fig. 23. Solving point (iv) with a single PD would be challenging, because it is hard to disaggregate colliding signals, a plausible alternative is to add more PDs with a narrower FoV to cover single lanes or tracks. Reducing the receivers' FoV would also help ameliorating point (v): a narrow FoV would allow us to use narrower stripes, which would increase the number of IDs that can be encoded on the object's surface. To alleviate point (vi), we can store the light intensity caused by ground reflection after calibration. When there is no object passing by and the ground reflection does not match with the stored value well, we can then recalibrate the orientation of transceivers.

VII. Conclusion

In this work, we took a first step to design a passive localization system based on visible light, where objects are not required to carry photosensors. To achieve our goal, we modify the external surfaces of objects so light reflections can provide information for localization and identification. We define and analyze the elements of our proposed system, and implement a testbed to benchmark its performance. Our results show that visible light can provide passive identification and localization with cm-level accuracy. Passive sensing and localization with visible light is a nascent area, we hope our work offers new insights in this up-and-coming domain.

Acknowledgements

We want to thank Danielle van der Werff for proposing the idea of using annular FoVs. She is working on it to provide 2D localization via light reflections for a swarm of robots. This work was supported in part by the Social Urban Data Lab (SUDL), Amsterdam Institute for Advanced Metropolitan Solutions (AMS), and the FWO SBO project SAMURAI.

References

[1] M. Wright, " Philips Lighting deploys LED-based indoor positioning in Carrefour hypermarket," *https://goo.gl/a0tGIj*, 2015.
[2] PureLiFi, *http://purelifi.com/*.
[3] G. Corbellini, "Connecting networks of toys and smartphones with visible light communication," *IEEE Communications Magazine*, 2014.
[4] E. Mok and G. Retscher, "Location determination using wifi fingerprinting versus wifi trilateration," *Journal of Location Based Services*, 2007.
[5] L. Li, P. Hu, C. Peng, G. Shen, and F. Zhao, "Epsilon: A visible light based positioning system," in *USENIX NSDI*, 2014.
[6] Y.-S. Kuo, P. Pannuto, and et. al., "Luxapose: Indoor positioning with mobile phones and visible light," in *ACM MobiCom*, 2014.
[7] Q. Wang, M. Zuniga, and D. Giustiniano, "Passive communication with ambient light," in *ACM CoNEXT*, 2016.
[8] L. Klaver and M. Zuniga, "Shine: a step towards distributed multi-hop visible light communication," in *IEEE MASS*, 2015.
[9] M. Youssef, M. Mah, and A. Agrawala, "Challenges: Device-free passive localization for wireless environments," in *MobiCom*, 2007.
[10] M. Moussa and M. Youssef, "Smart cevices for smart environments: Device-free passive detection in real environments," in *PerCom*, 2009.
[11] F. Adib, Z. Kabelac, and D. Katabi, "Multi-person localization via RF body reflections," in *USENIX NSDI*, 2015.
[12] I. Sabek and et al, "ACE: An accurate and efficient multi-entity device-free WLAN localization system," *IEEE Trans. TMC.*, 2015.
[13] Z. Yang and et. al., "Wearables can afford: Light-weight indoor positioning with visible light," in *ACM MobiSys*, 2015.
[14] B. Xie, S. Gong, and G. Tan, "LiPro: light-based indoor positioning with rotating handheld devices," *Wireless Networks*, 2016.
[15] J. R. Barry, *Wireless infrared communications*. Springer, 1994.
[16] C. Zhang, J. Tabor, J. Zhang, and X. Zhang, "Extending mobile interaction through near-field visible light sensing," in *MobiCom*, 2015.
[17] Y. Yang *et al.*, "Ceilingsee: Device-free occupancy inference through lighting infrastructure based led sensing," in *PerCom*, 2017.
[18] E. D. Lascio *et al.*, "Poster abstract: Localight - a battery-free passive localization system using visible light," in *IPSN*, 2016.